# CIS-LUNAR ORBIT DETERMINATION SENSITIVITY ANALYSIS WITH REFERENCE TO OBSERVATIONAL GEOMETRY

# James McElreath, Manoranjan Majji† Texas A & M University, College Station, TX, 77843-3141

The sensitivity of the initial condition [epoch state] orbit determination program with respect to ranging geometry is studied in this paper. Using the nonlinear least squares orbit determination program with representative dynamics and sensor models, the effects of operational considerations, such as the drop of regular ranging, information are studied. A representation of the linearized error covariance of the epoch state as a function of observation epoch is presented to provide a visual inspection of the relative measures of accuracy of the state. Applications of this analysis are applied to an orbit estimation problem, whereby the orbit of an artificial satellite around the Moon is estimated using range and range rate observations from sites located on the Earth. Information-gain measures are presented to reveal optimal observation epochs and the influence of observational geometry. Comparisons are made between information-gain profiles determined from true measurement data and measurement data generated from *a priori* estimates.

# INTRODUCTION

Uncertainty analysis forms the cornerstone of all aspects of modern nonlinear systems analysis. Sophisticated tools for modeling, propagation and data assimilation of uncertain dynamical systems have been developed and incorporated into engineering practice in the past three decades. <sup>1–4</sup> This is particularly true in astrodynamics, where the evolution laws are well-known and the sparse measurement rates allow nonlinear transformations of prior probability density function (PDF) to invalidate the Gaussian assumption made by the Kalman filter and its related formulations.

One of the most important physical problems with precise dynamical models and sparse measurements is that of space object tracking. Junkins recognized the importance of non-Gaussian error propagation in orbital mechanics.<sup>5,6</sup> While originally considered of academic interest, the advent of Kessler syndrome and allied quests to enhance space situational awareness (SSA) has recently brought extensive attention to the important problem of Non-Gaussian error propagation through dynamical systems.<sup>7–11</sup> Accurate state and uncertainty information play an important role for satellites in the cis-lunar domain. Applications such lunar surface mapping, land and descent operations, collision prevention, and proximity operations all rely on state estimates and the associated uncertainty. In addition to the uncertainties associated with the state estimate derived from observations of the satellite, space applications typically necessitate the inclusion of parametric uncertainties associated with the parameters of the dynamical model.<sup>12–14</sup>

As with any other nonlinear state estimation problem, the measurement sparsity, nonlinearity of the ranging process, measurement accuracy of the sensor system, and the model uncertainty of the

<sup>\*</sup>Graduate Research Assistant, Land, Air and Space Robotics (LASR) Laboratory, Aerospace Engineering

<sup>&</sup>lt;sup>†</sup>Assistant Professor, Director, Land, Air and Space Robotics (LASR) Laboratory, Aerospace Engineering

satellite motion with respect to the observation station influence the ultimate accuracy of the state estimation process. He to quantify the effects of these elements on the ultimate accuracy of the batch or sequential estimation method and the associated state uncertainty are studied in the literature. Measurement geometry plays an important role in the ultimate accuracy of the epoch state of interest. Other than the well-known geometric dilution of precision in the GPS-INS literature, the research literature does not offer many approaches to carryout sensitivity analysis of the accuracy of the state estimator (or the variance of the estimator) with respect to the parameters that influence the geometry of the observation process. The goal of this paper is the determine optimal observation epochs as well as the influence of observational geometry on state uncertainty and information-gain. This is important, as observation measurements of satellites in the in the lunar domain are usually made in short burst with significant breaks in-between. Therefore, ways to maximize the limited observation window are useful during mission and operation planning.

# **ORBIT DETERMINATION PROBLEM**

Before studying the sensitivity of epoch state orbit determination, let us define the state determination problem considered in this paper. The problem considered aims to update the estimated epoch state parameters (initial conditions) of a chosen lunar orbiter from ground-based Earth observations. Dynamic models are used to integrate state estimates and uncertainties at epoch to each observation time, yielding predicted observations. The differences between the predicted and measured observations are defined to be the residual error. Finally, the current epoch state estimate is recursively updated to minimize the sum squared value of the residuals. Therefore, a dynamic model of the cis-lunar space and a measurement model of ground-based Earth observations are required.

# **Dynamic Model**

To generate ephemeris data of a lunar orbiter, linearized equations of motion of a satellite in cis-lunar domain are derived and then numerically integrated over the time-region of interest. The equations of motion are derived with respect to an inertial frame centered at the Moon's origin. The equations on motion are given in equations 1 and 2, where  $\bf r$  denotes the position vector,  $\bf v$  denotes the velocity vector, and dot notation above a variable denotes the time derivative in an inertial frame. The dynamic model implemented accounts for the three largest gravitational perturbing effects that act on a satellite in the cis-lunar domain: Earth ( $\bf g_{Earth}$ ), Sun ( $\bf g_{Sun}$ ), and Moon ( $\bf g_{Moon}$ ) gravitational accelerations. Acceleration of the frame origin ( $\bf a_{origin}$ ) is removed to ensure proper dynamic modeling. The Moon gravitational acceleration is modeled using the NASA developed GRAIL660B model, while the Earth and Sun gravitational accelerations are assumed to be point mass models. Solar-radiation-pressure and drag effects are not considered. The reasoning being that they are both difficult to accurately model (due to randomness of the projected normal area) and cause significantly less of a perturbing effect when compared against the gravitational accelerations. This greatly reduces the complexity of the three-body problem while still retaining the primary perturbing effects that are experienced in the cis-lunar domain.

$$\dot{\mathbf{r}} = \mathbf{v} \tag{1}$$

$$\dot{\mathbf{v}} = \mathbf{g}_{Moon} + \mathbf{g}_{Earth} + \mathbf{g}_{Sun} - \mathbf{a}_{origin} \tag{2}$$

### **Measurement Model**

For the state estimation process, range and range-rate measurements are utilized from ground-based Earth sites. The geometry of the problem considered is found in figure 1. Range  $(\rho)$  is

calculated as the magnitude of the line-of-sight vector ( $\rho$ ). The line-of-sight vector is generated from three position vectors: lunar-satellite with respect to Moon-center ( $\mathbf{r}$ ), Moon-center with respect Earth-center ( $\mathbf{R}$ ), and ground-site with respect to Earth-center ( $\mathbf{S}$ ). Range-rate ( $\dot{\rho}$ ) is calculated as the component of line-of-sight vector time-derivative ( $\dot{\rho}$ ) that lies along the line-of-sight vector. The line-of-sight vector time-derivative is generated from the line-of-sight vector, the time-derivatives of  $\mathbf{R}$  and  $\mathbf{S}$ , and the satellite velocity ( $\mathbf{v}$ ). Formal definitions of the range and range-rate (taken in an inertial frame) are given by the equations 3 and 4, respectively. Range and range-rate measurements are assumed unavailable if line-of-sight is broken. Two considerations for the breaking of line-of-sight are made in the current measurement model: the Moon blocks line-of-sight and the line-of-sight vector is not within the ground site's visibility-cone. Vector geometry is leveraged in both cases to determine when Earth ground-based communications are achievable.

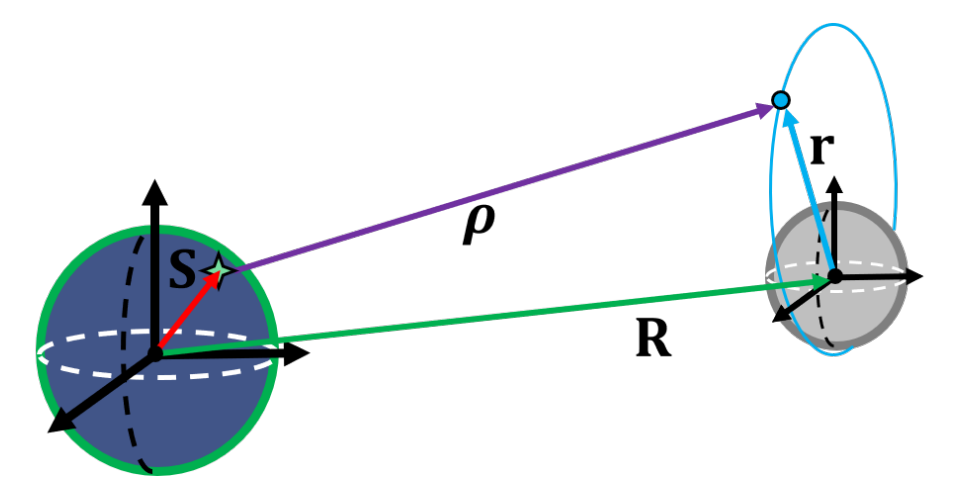


Figure 1. Geometry of an epoch state estimation problem from ground based observations

$$\rho = |\boldsymbol{\rho}| = |\mathbf{r} + \mathbf{R} - \mathbf{S}| \tag{3}$$

$$\dot{\rho} = \dot{\boldsymbol{\rho}} \cdot \frac{\boldsymbol{\rho}}{|\boldsymbol{\rho}|} = (\mathbf{v} + \dot{\mathbf{R}} - \dot{\mathbf{S}}) \cdot \frac{\boldsymbol{\rho}}{|\boldsymbol{\rho}|}$$
(4)

Figure 2 reveals the vector geometry utilized to determine when the Moon blocks line-of-sight. A new vector,  $\mathbf{d}$ , is defined based on the minimum-distance between the line-of-sight vector and the center of the Moon. The magnitude of this minimum-distance vector is determined using equation 5, where  $\theta$  is the angle between  $\rho$  and  $\mathbf{r}$ . Once the magnitude of  $\mathbf{d}$  drops below the distance between the Moon's surface and center, the line-of-sight is blocked. To simplify, the Moon is assumed to be perfectly spherical. This results in line-of-sight breaking when the magnitude of  $\mathbf{d}$  drops below the equatorial radius of the Moon. Figure 3 reveals the vector geometry utilized to determine whether the line-of-sight vector is within the ground site's visibility-cone. The angle  $\psi$  is calculated by equation 6 and is defined as the angle between the site vector  $\mathbf{S}$  and the range vector  $\rho$ . The lunar-satellite will be within the site's visibility-cone while  $\psi$  remains below the site's visibility-cone half angle  $(\phi)$ .

$$d = |\mathbf{d}| = r \cdot \sin \theta = |\mathbf{r}| \cdot \sin \left( \arccos \left( \frac{\mathbf{r} \cdot \boldsymbol{\rho}}{|\mathbf{r}||\boldsymbol{\rho}|} \right) \right)$$
 (5)

$$\psi = \arccos\left(\frac{\mathbf{S} \cdot \boldsymbol{\rho}}{|\mathbf{S}||\boldsymbol{\rho}|}\right) \tag{6}$$

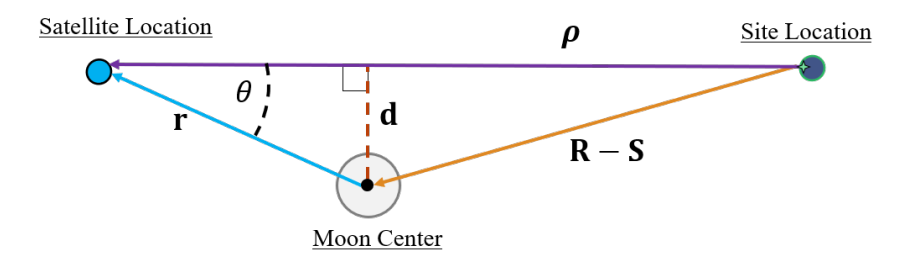


Figure 2. Two-dimensional triangle to illustrate when Moon blocks line-of-sight

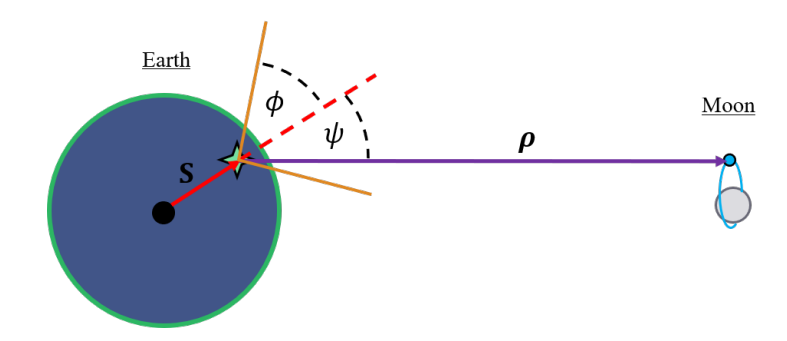


Figure 3. Figure to illustrate when line-of-sight is within the site visibility-cone

# **BATCH ESTIMATION ALGORITHM**

To perform a sensitivity analysis on the accuracy and variance of state estimates, the implementation of either a sequential or batch estimation process is required. Continuous communication between a satellite in cis-lunar domain and an Earth-bound site is not practical due to effects such as eclipsing, line-of-sight blocking, and communication expense budgets. This causes lunar missions to implement short measurement periods (on the order of tens of minutes) when attempting data collection for the state estimation problem. Significant down-times (on the order of days) are expected between measurement samplings, allowing for the use of a batch estimation process to update the current epoch state estimate. Thus, a batch estimation algorithm that accounts for *a priori* estimates and uncertainties will be used to perform the sensitivity analysis on the estimation of epoch states.

# **Nonlinear Least Squares Estimation**

This section presents the nonlinear least squares implemented for the batch estimator. The notation of the nonlinear least squares estimator is that of Crassidis and Junkins. For the derivations, it is recommend that the reader see the *Optimal Estimation of Dynamic Systems* textbook. <sup>16</sup> Equation 7 defines the epoch state vector as the position-velocity vectors in a Moon-centered inertial frame ( $\mathbf{x}_0$ ) at the time of epoch ( $t_0$ ).

$$\mathbf{x}_0 = \mathbf{x}(t_0) = [\mathbf{r}_0^T \ \mathbf{v}_0^T]^T \tag{7}$$

Equation 8 defines the measurements as the *a priori* epoch estimate  $(\mathbf{x}_0^a)$ , range observations  $(\tilde{\rho})$ , and the range-rate observations  $(\tilde{\rho})$ .

$$\tilde{\mathbf{y}} \equiv \begin{bmatrix}
\mathbf{x}_0^a \\ \tilde{\rho}(t_1) \\ \tilde{\rho}(t_1) \\ \vdots \\ \tilde{\rho}(t_N) \\ \tilde{\rho}(t_N)
\end{bmatrix}$$
(8)

Equation 9 defines the measurement function, where  $\hat{\mathbf{x}}_0$  is the epoch state estimate.

$$\mathbf{f}(\hat{\mathbf{x}}_0) \equiv \begin{bmatrix} \hat{\mathbf{x}}_0 \\ \rho(\hat{\mathbf{x}}_0, t_1) \\ \dot{\rho}(\hat{\mathbf{x}}_0, t_1) \\ \vdots \\ \rho(\hat{\mathbf{x}}_0, t_N) \\ \dot{\rho}(\hat{\mathbf{x}}_0, t_N) \end{bmatrix}$$
(9)

Because the range and range-rate are determined from nonlinear functions of the epoch state vector, a first order Taylor series approximation is used to linearize about the current epoch state estimate  $(\mathbf{x}_0^c)$  with an unknown update  $(\Delta \mathbf{x}_0)$ .

$$\tilde{\mathbf{y}} = \mathbf{f}(\hat{\mathbf{x}}_0) + \mathbf{e} = \mathbf{f}(\mathbf{x}_0^c) + H\Delta\mathbf{x}_0 + \mathbf{e}$$
(10)

where

$$H \equiv \left. \frac{\partial \mathbf{f}}{\partial \mathbf{x}_0} \right|_{\mathbf{x}_0^c} \tag{11}$$

The gradient matrix H is known as the *Jacobian* and the vector  $\mathbf{e}$  is known as the residual errors. The cost function can now defined as the weighted sum squared of the residual errors:

$$J = \frac{1}{2} \mathbf{e}^T W \mathbf{e} = \frac{1}{2} [\tilde{\mathbf{y}} - \mathbf{f}(\mathbf{x}_0^c) - H\Delta \mathbf{x}_0]^T W [\tilde{\mathbf{y}} - \mathbf{f}(\mathbf{x}_0^c) - H\Delta \mathbf{x}_0]$$
(12)

The cost function is then minimized to determine the update to the current epoch state estimate:

$$\Delta \mathbf{x}_0 = (H^T W H)^{-1} H^T W (\tilde{\mathbf{y}} - \mathbf{f}(\mathbf{x}_0^c))$$
(13)

The process is initialized with the *a priori* estimated, and is then repeated with the each new estimate until the following convergence criterion is met:

$$\delta J \equiv \frac{|J(\mathbf{x}_0^c + \Delta \mathbf{x}_0) - J(\mathbf{x}_0^c)|}{J(\mathbf{x}_0^c + \Delta \mathbf{x}_0)} < \frac{\gamma}{|W|}$$
(14)

where  $\gamma$  is some prescribed small value.

# **Optimal Weight Matrix**

It is known that setting the weight matrix W equal to the inverse of the observation covariance matrix R will yield the minimal variance estimate. For the considered orbit determination problem, the optimal weight matrix is given by:

$$W \equiv R^{-1} = \begin{bmatrix} P_a & O(6 \times 2) & \cdots & O(6 \times 2) \\ O(2 \times 6) & P_r(t_1) & \cdots & O(2 \times 2) \\ \vdots & \vdots & \ddots & \vdots \\ O(2 \times 6) & O(2 \times 2) & \cdots & P_r(t_N) \end{bmatrix}^{-1}$$
(15)

The matrix  $P_a$  is the covariance matrix associated with the *a priori* epoch state estimate. The matrix O is the zero matrix following the notation such that  $(n \times m)$  yields a matrix of n rows by m columns. The matrix  $P_r$  is the range and range-rate measurement covariance matrix and is given as

$$P_r(t) = P_r = \begin{bmatrix} (\sigma_\rho)^2 & 0\\ 0 & (\sigma_{\dot{\rho}})^2 \end{bmatrix}$$
 (16)

where  $\sigma_{\rho}$  and  $\sigma_{\dot{\rho}}$  are the one standard deviation measurement white-noises of the range and rangerate measurements, respectively. With the optimal weight matrix defined, the calculation of the covariance matrix of the current epoch state estimate is made by the following equation:

$$P_c = \left( H^T W H \right)^{-1} \Big|_{\mathbf{x}_0^c} \tag{17}$$

# **Measurement Function Partials**

First order partials of the epoch state, range observations, and range-rate observations with respect to the epoch state are given by:

$$\frac{\partial \mathbf{x}_0}{\partial \mathbf{x}_0} = I(6 \times 6) \tag{18}$$

$$\frac{\partial \rho(t)}{\partial \mathbf{x}_0} = \frac{\partial \rho}{\partial \mathbf{x}(t)} \frac{\partial \mathbf{x}(t)}{\partial \mathbf{x}_0} = \frac{1}{\rho} \begin{bmatrix} \boldsymbol{\rho}^T & 0 & 0 & 0 \end{bmatrix} \frac{\partial \mathbf{x}(t)}{\partial \mathbf{x}_0}$$
(19)

$$\frac{\partial \dot{\rho}(t)}{\partial \mathbf{x}_0} = \frac{\partial \dot{\rho}}{\partial \mathbf{x}(t)} \frac{\partial \mathbf{x}(t)}{\partial \mathbf{x}_0} = \frac{1}{\rho} \left[ \left( 1 - \frac{(\boldsymbol{\rho} \cdot \dot{\boldsymbol{\rho}})}{\rho^2} \right) \boldsymbol{\rho}^T \quad \boldsymbol{\rho}^T \right] \frac{\partial \mathbf{x}(t)}{\partial \mathbf{x}_0}$$
(20)

where

$$\frac{\partial \mathbf{x}(t)}{\partial \mathbf{x}_0} \equiv \Phi(t, t_0) \tag{21}$$

The matrix  $\Phi$  is known as the State Transition Matrix and is used to approximate the partials of the state at the current measurement time,  $\mathbf{x}(t)$ , with respect to the epoch state. Since the considered perturbing accelerations in the problem are all deterministic analytical functions, the state transition matrix is calculated using numerical integration. The state transition matrix is propagated in tandem with the epoch state estimate to each of the measurement times. This means no numerical differentiation methods are required when calculating the Jacobian, greatly reducing the computation load when performing the estimation process. This is important as the sensitivity analysis, shown later on, will require many successive estimation computations over a range of observation epochs.

An analytical solution to the state transition matrix is not known for this problem. Therefore, numerical integration of differential equations derived from the equations of motion are used to determine the state transition matrix at each time of observation.

$$\frac{d}{dt}\Phi(t,t_0) = F(t)\Phi(t,t_0); \qquad \Phi(t_0,t_0) = I(6 \times 6)$$
(22)

where

$$F(t) = \begin{bmatrix} O(3 \times 3) & I(3 \times 3) \\ G(t) & O(3 \times 3) \end{bmatrix}$$
 (23)

and

$$G(t) = \frac{\partial \mathbf{g}}{\partial \mathbf{r}}\Big|_{\mathbf{r}(t)} = \left[ \frac{\partial \mathbf{g}_{Moon}}{\partial \mathbf{r}} + \frac{\partial \mathbf{g}_{Earth}}{\partial \mathbf{r}} + \frac{\partial \mathbf{g}_{Sun}}{\partial \mathbf{r}} \right]\Big|_{\mathbf{r}(t)}$$
(24)

As stated earlier, the Sun and Earth gravitational accelerations are modeled as point masses. The equation for their perturbing accelerations are given as follows:

$$\mathbf{g}_{Earth} = -\frac{\mu_{Earth}}{|\mathbf{r} + \mathbf{R}|^3} (\mathbf{r} + \mathbf{R})$$
 (25)

$$\mathbf{g}_{Sun} = -\frac{\mu_{Sun}}{|\mathbf{r} + \mathbf{R}_{Moon/Sun}|^3} (\mathbf{r} + \mathbf{R}_{Moon/Sun})$$
 (26)

and their first order partials:

$$\frac{\partial \mathbf{g}_{Earth}}{\partial \mathbf{r}} = -\frac{\mu_{Earth}}{|\mathbf{r} + \mathbf{R}|^3} \cdot I(3 \times 3) + 3\mu_{Earth} \frac{(\mathbf{r} + \mathbf{R}) \cdot (\mathbf{r} + \mathbf{R})}{|\mathbf{r} + \mathbf{R}|^5}$$
(27)

$$\frac{\partial \mathbf{g}_{Sun}}{\partial \mathbf{r}} = -\frac{\mu_{Sun}}{|\mathbf{r} + \mathbf{R}_{Moon/Sun}|^3} \cdot I(3 \times 3) + 3\mu_{Sun} \frac{(\mathbf{r} + \mathbf{R}_{Moon/Sun}) \cdot (\mathbf{r} + \mathbf{R}_{Moon/Sun})}{|\mathbf{r} + \mathbf{R}_{Moon/Sun}|^5}$$
(28)

where  $\mathbf{R}_{Moon/Sun}$  is the position vector that points from Sun-center to Moon-center. The Moon gravitational acceleration is modeled using the Lunar GRAIL660B model, with a model order of  $160 \times 160$  used for all calculations in this paper. The NASA contractor report written by Robert G. Gottlieb<sup>18</sup> gives the gravitational potential function as

$$V = -\frac{\mu_{Moon}}{r} - \sum_{n=2}^{\infty} \sum_{m=0}^{n} \frac{\mu_{Moon}}{r} \left(\frac{r_e}{r}\right)^2 P_{n,m}(\varepsilon) \left(C_{n,m}\cos\left(m\lambda\right) + S_{n,m}\sin\left(m\lambda\right)\right)$$
(29)

where  $r_e$  is the Moon equatorial radius,  $C_{n,m}$  and  $S_{n,m}$  are the unnormalized cosine and sine gravity coefficients that result from the mass distribution of the Moon, and

$$P_{n,m} = (1 - \varepsilon^2)^{\frac{m}{2}} \left( \frac{\partial^m P_n}{\partial \varepsilon^m} \right)$$
 (30)

are the associated Legendre functions and  $P_n$  are the Legendre polynomials. Also, the sine of latitude is given by

$$\varepsilon = \frac{r_3}{r} \tag{31}$$

and the longitude is computed from

$$\tan \lambda = \frac{r_2}{r_1} \tag{32}$$

where

$$\mathbf{r}_f = [r_1, r_2, r_3]^T \tag{33}$$

is the Moon-fixed position vector. The first order partial of the gravitational potential function with respect to the Moon-fixed position vector yields the gravitational acceleration in the Moon-fixed frame. This acceleration is then converted to the Moon-centered inertial frame in equation 34 by use of the rotation matrix C. The second order partial yields the first order partial of gravitational acceleration with respect to the Moon-fixed position vector in the Moon-fixed frame. This acceleration partial is then converted to the Moon-centered inertial frame in equation 35 by use of the rotation matrix C. The derivations and calculation methods of these partials are found in the NASA contractor report.<sup>18</sup>

$$\mathbf{g}_{Moon} = C\left(-\frac{\partial V}{\partial \mathbf{r}_f}\right) \tag{34}$$

$$\frac{\partial \mathbf{g}_{Moon}}{\partial \mathbf{r}} = C \left( -\frac{\partial^2 V}{\partial \mathbf{r}_f^2} \right) C^T \tag{35}$$

#### SENSITIVITY ANALYSIS

#### **Problem Formulation**

For the sensitivity analysis of epoch state orbit determination problem, two scenarios are considered. Each scenario is assumed to have the same *a priori* epoch state estimate and associated covariance matrix at a given epoch time. The *a priori* epoch state estimate and covariance matrix is generated from an initializing orbit determination problem. The estimated epoch state and covariance matrix will be updated with the batch estimation algorithm detailed in this paper using observations sampled over a range of observation epochs. Observations are generated from multiple ground sites, with the intent of the analysis to reveal optimal ground-sites and observation epochs with regards to information-gain of the epoch state uncertainty. In the first scenario, ephemeris data used to generate observation measurements are simulated using the true epoch state. In the second scenario, ephemeris data used to generate observation measurements are simulated using the *a priori* epoch state estimate.

With truth information available, the true epoch state and estimated epoch state can be used to generate Mahalanobis distance and compare against linearized uncertainties against the errors to evaluate the statistical consistency of the batch estimator. In real-world missions, true state information is never known due to inherent noises associated with measurements and dynamical models. In spite of this, the true state information is assumed known to provide the true observation measurements to batch estimator in Scenario 1 and allow for error determination. This will act as the "truth data" of what is to be expected when observations are performed at different observation epochs in the future. This data will be compared against information-gain profiles generated in scenario two, with the intent being to show that the information-gain profiles are stable between scenarios.

When generating range and range-rate measurements from an *a priori* epoch state estimate, measurements will have uncertainty aside from the measurement white-noise. This additional uncertainty must be included in the batch estimator to ensure properly weighting of the measurement data. To do this, uncertainty in the epoch state is transformed to the range and range-rate space at the observation time and then added to the measurement white-noise covariance matrix. An updated version of equation 16 is provided by utilizing the range partial with respect to the current

state (equation 19), the range-rate partial with respect to the current state (equation 20), the state transition matrix (equation 21), and the *a priori* epoch state covariance matrix:

$$P_r(t) = \begin{bmatrix} (\sigma_{\rho})^2 & 0\\ 0 & (\sigma_{\dot{\rho}})^2 \end{bmatrix} + \begin{bmatrix} \frac{\partial \rho}{\partial \mathbf{x}(t)}\\ \frac{\partial \dot{\rho}}{\partial \mathbf{x}(t)} \end{bmatrix} \Phi(t, t_0) P_a \Phi(t, t_0)^T \begin{bmatrix} \frac{\partial \rho}{\partial \mathbf{x}(t)}\\ \frac{\partial \dot{\rho}}{\partial \mathbf{x}(t)} \end{bmatrix}^T$$
(36)

Two lunar orbits are considered for the sensitivity analysis; an eccentric lunar-polar orbit and a near-circular lunar-equatorial orbit. The Moon Principal Axis orbital elements at the analysis epoch (1 Jan 2020 00:00:00.000 UTCG) of each are given in table 1. To provide a priori state and uncertainty information for each orbit at the analysis epoch, an initializing orbit determination problem is solved using continuous, true measurement data over three orbits from the start of the analysis. The state estimates and uncertainties are propagated approximately five days forward in time to a new epoch location, the scenario epoch. This allows for the covariance matrices to grow and mimics the down-time between ground-based communications. The determined state uncertainties at the scenario epoch for Orbit 1 are on the order of 10s of meters in the position space and 10s of millimeters per second in the velocity space. The determined state uncertainties for Orbit 2 at the scenario epoch are on the order of 100s of meters in the position space and 10s of centimeters per second in the velocity space. Note, previous analyses have illustrated that 10s of meters of position uncertainty and 10s of millimeters per second of velocity uncertainty is expected when using ranging observations in the lunar domain. 19-22 Uncertainty values for Orbit 2 are purposely higher to show that conclusions drawn on the stability of information-gain profiles still apply with large a priori epoch state uncertainty. The epoch state estimate and covariance matrix at the scenario epoch are used as the a priori information ( $\mathbf{x}_0^a$  and  $P_a$ ) for both scenarios in the sensitivity analysis.

Table 1. Moon Principal Axis orbital elements at analysis epoch

a	e	Ω	i	ω	M
3,800 km 3,800 km			90°	270° 90°	0°

A 12 hour communication window starting at the scenario epoch is implemented for the sensitivity analysis. Ground-based sites are employed to provide observations sets at three different locations: Kiruna Sweden, Weilheim Germany, and NASA's Johnson Space Center (JSC). Each of these sites is subject to measurement model restrictions detailed in the *Measurement Model* section of this paper, with each site designated a generous visibility-cone half angle of sixty degrees to provide a large range of observation sets. A fourth observation location is set to the Earth-center, and is not subject to the measurement restrictions of the ground-based sites. Earth-centered observations will act as a control and fill in the uncertainly profiles when no ground-based sites can observe the satellite. All observation locations are a configured with 5 meters of range measurement noise  $(\sigma_{\rho})$  and 5 millimeters per second of range-rate measurement noise  $(\sigma_{\dot{\rho}})$ , values that are of the same order of magnitude Lunar Reconnaissance Orbiter (LRO) tracking data. <sup>19–22</sup>

During the communication window, 30 minute sampling durations are employed to provide range and range-rate observation data. Samplings are performed for each observation location every 15

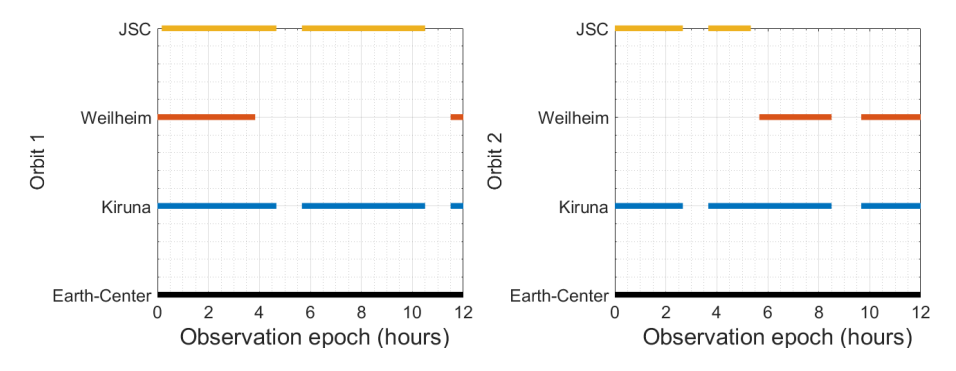


Figure 4. Observation location access time figure

minutes from the start of the scenario epoch, assuming that communications are available over the entire sampling duration. The time at which the sampling begins is stated to be the observation epoch. The observation timestep during the sampling window is configured to 20 seconds. Each of the 30 minute samplings are run through the batch estimation algorithm to provide an updated epoch state estimate  $(\mathbf{x}_0^p)$  and covariance matrix  $(P_p)$  at the scenario epoch. This *a posteriori* information is then plotted as function of the observation epoch (measured in time from scenario epoch) to show uncertainty profiles and reveal optimal observation times during the communication window. Access times for each observation location is given in figure 4, with the left side showing access times for Orbit 1 and right side showing access times for Orbit 2. If the color bars are present, the ground-site communication is assumed available. The small breaks in the profiles are due to Moon blocking line-of-sight and the large breaks due to the line-of-sight vector not being within the sites visibility-cone.

In an effort to make the optimal observation epoch more apparent, measures of position, velocity, and general information-gain are presented. The measure of position information-gain  $(IG_p)$  is generated by dividing the volume of the  $1\sigma$  a posteriori position covariance ellipsoid by the volume of the  $1\sigma$  a priori position covariance ellipsoid. Position covariance ellipsoid volumes are calculated by taking the eigenvalues of the top-left  $3\times 3$  elements of the associated covariance matrix and multiplying the square-root of each eigenvalue together. This position information-gain measure will reveal by how much the position covariance ellipsoid has shrunk due to the new observations. The measure of velocity information-gain  $(IG_v)$  is generated in the same manner as the position measure, except that the eigenvalues are calculated from the bottom-right  $3\times 3$  elements of the associated covariance matrix. The measure of general information-gain  $(IG_g)$  is generated in the same manner as the position and velocity measure, except that the eigenvalues are calculated from the entire  $6\times 6$  covariance matrix. The position, velocity, and general information-gain measures are given by equations 37, 38, and 39, respectfully.

$$IG_p = \frac{\prod \left(eig(P_p(1:3,1:3))^{1/2}\right)}{\prod \left(eig(P_a(1:3,1:3))^{1/2}\right)}$$
(37)

$$IG_v = \frac{\prod \left(eig(P_p(4:6,4:6))^{1/2}\right)}{\prod \left(eig(P_a(4:6,4:6))^{1/2}\right)}$$
(38)

$$IG_g = \frac{\prod \left(eig(P_p)^{1/2}\right)}{\prod \left(eig(P_a)^{1/2}\right)}$$
(39)

Since true state information is assumed in Scenario 1, the Mahalanobis distance between the *a posteriori* epoch state ( $\mathbf{x}_0^p$ ) and the true epoch state is attainable. In this analysis, Mahalanobis distance is used to determine a multi-dimensional generalized measure of how many standard deviations away the epoch state estimate is from the true epoch state. Inspecting the Malahanobis distance of the estimated state will reveal the accuracy of the determined epoch state uncertainty. The Mahalanobis distance of the epoch state is calculated by equation 40. It is expected that Mahalanobis distance should be around a value of one, indicating that the epoch state estimate is approximately one standard deviation from the true epoch state.

$$D_M = \sqrt{(\mathbf{x}_0^p - \mathbf{x}_0)^T (P_p)^{-1} (\mathbf{x}_0^p - \mathbf{x}_0)} / 6$$
(40)

### Results

Figure 5 reveals the convergence error of the a posteriori epoch state and associated linearized  $3\sigma$  standard deviation at the scenario epoch time as a function of the observation epoch for Orbit 1. The figure reveals each of the six states of the epoch state vector expressed in the orbital plane coordinate system. This has been done because the directions of the orbital plane unit-vectors are the most intuitive for states expressed at epoch location. Each error point is represented by a scatter plot dot, while the linearized  $3\sigma$  bounds are represented by dashed lines. It is seen that the uncertainty profiles fluctuate over the communications window, indicating different levels of observability for each observation epoch. It is also seen that the uncertainty profiles are similar between each of the observation locations, indicating similar levels of observability for each site over the communications window. There is slight bias in the convergence error, which is expected due to the use of a priori information in the batch estimation algorithm. Convergence errors at all observation epochs are seen to be within the linearized  $3\sigma$  bounds, indicating statistical consistency of the a posteriori estimates produced by the batch estimation algorithm. This consistency is further bolstered by figure 6, where the Mahalanobis distance of the Orbit 1 a posteriori epoch state estimates are shown. Values of the Mahalanobis distance are seen to be scattered around a value of one, indicating the accuracy of the *a posteriori* epoch state uncertainty information.

Figure 7 reveals the information-gain measures as a function of the observation epoch for Orbit 1. Information-gains for Scenario 1 are found on the left side and Scenario 2 on the right. From visual inspection, it is seen that the two profiles are near identical between scenarios. This indicates that a priori epoch estimates used to generate simulated measurement observations will reveal the same optimal observation epoch as determined from what would be true observation data. It is also seen that each information-gain measure reveals only slight variations between each observation location. This is expected, as little variation was seen between the linearized  $3\sigma$  uncertainty profiles. It should be noted how the general information-gain measure profile behaves similar to an averaging of the position and velocity information-gain. It is seen that minimums of each measure occur at similar observation epochs (observation epoch times of 6 and 12 hours). This shows that the general information-gain measure captures the uncertainty of the entire epoch state. The optimal observation epoch and ground-site is then selected based on position, velocity, or general information-gain priority.

From visual inspection of figure 8, it is seen that the variations of range and range-rate over the observation period affect the information-gain. The variations in range and range-rate were calculated by taking the line-integral of the measurement data over the sampling period and then dividing by the duration of the sampling period. It is seen that smaller variations in the range

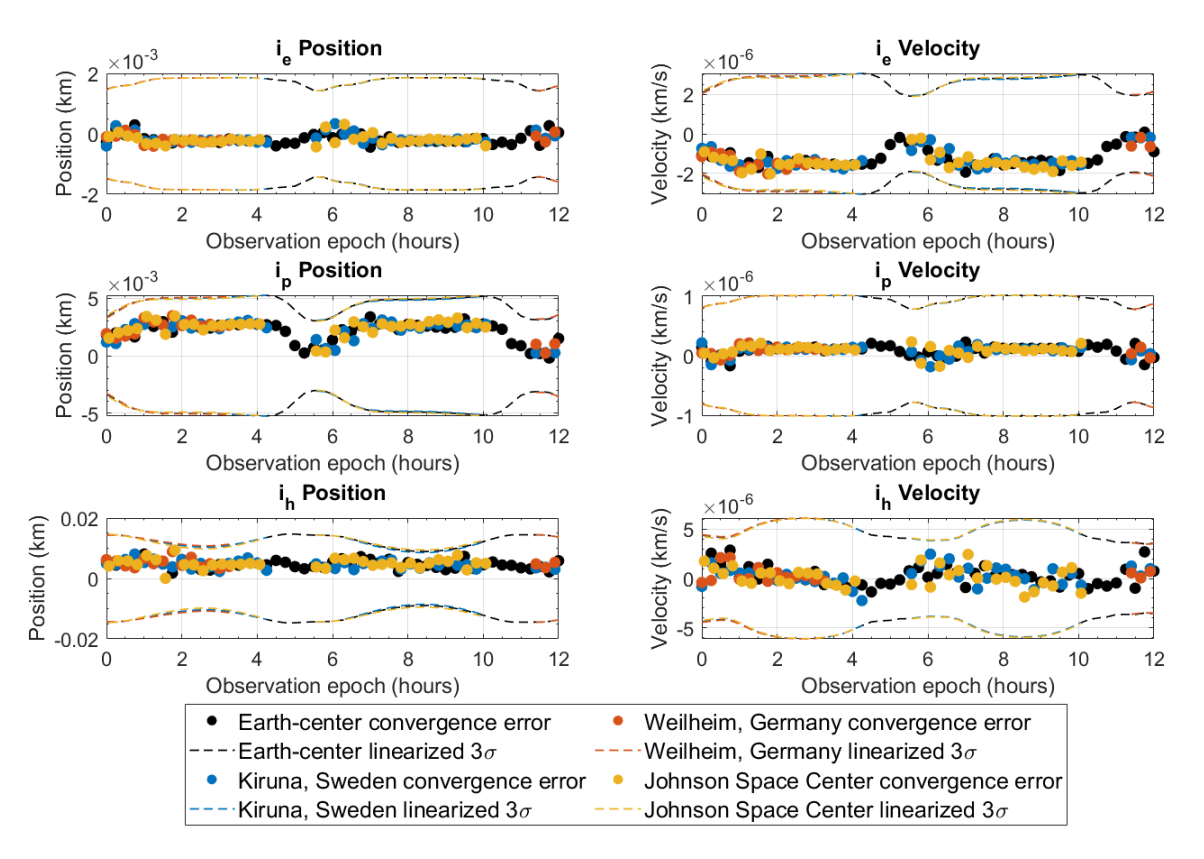


Figure 5. Orbit 1 convergence error and linearized  $3\sigma$  uncertainty bounds

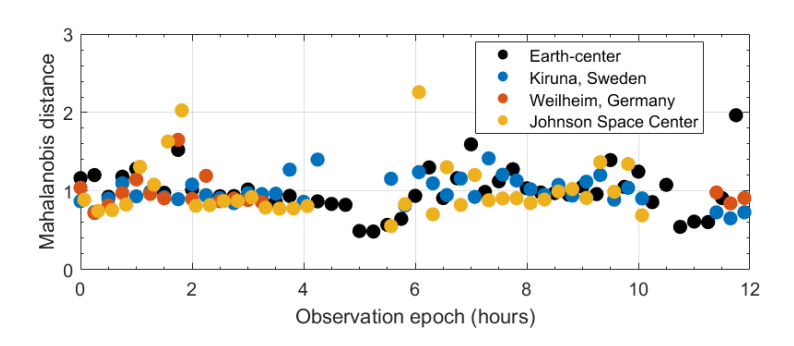


Figure 6. Orbit 1 Mahalanobis distance

measurements yield larger values in position information-gain. It is also seen that smaller variations in the range-rate measurements yield larger values in velocity information-gain. Unsurprisingly, this implies that more variation in the measurement data leads to more observability in the epoch state orbit determination problem. There are slight differences in the profiles of information-gain between observation location, but it is measurement variation is the driving parameter of the observability for Orbit 1.

Figure 9 reveals the convergence error of the *a posteriori* epoch state and associated linearized  $3\sigma$  standard deviation at the scenario epoch time as a function of the observation epoch for Orbit 2. Once again, convergence errors at all observation epochs are seen to be within their respective

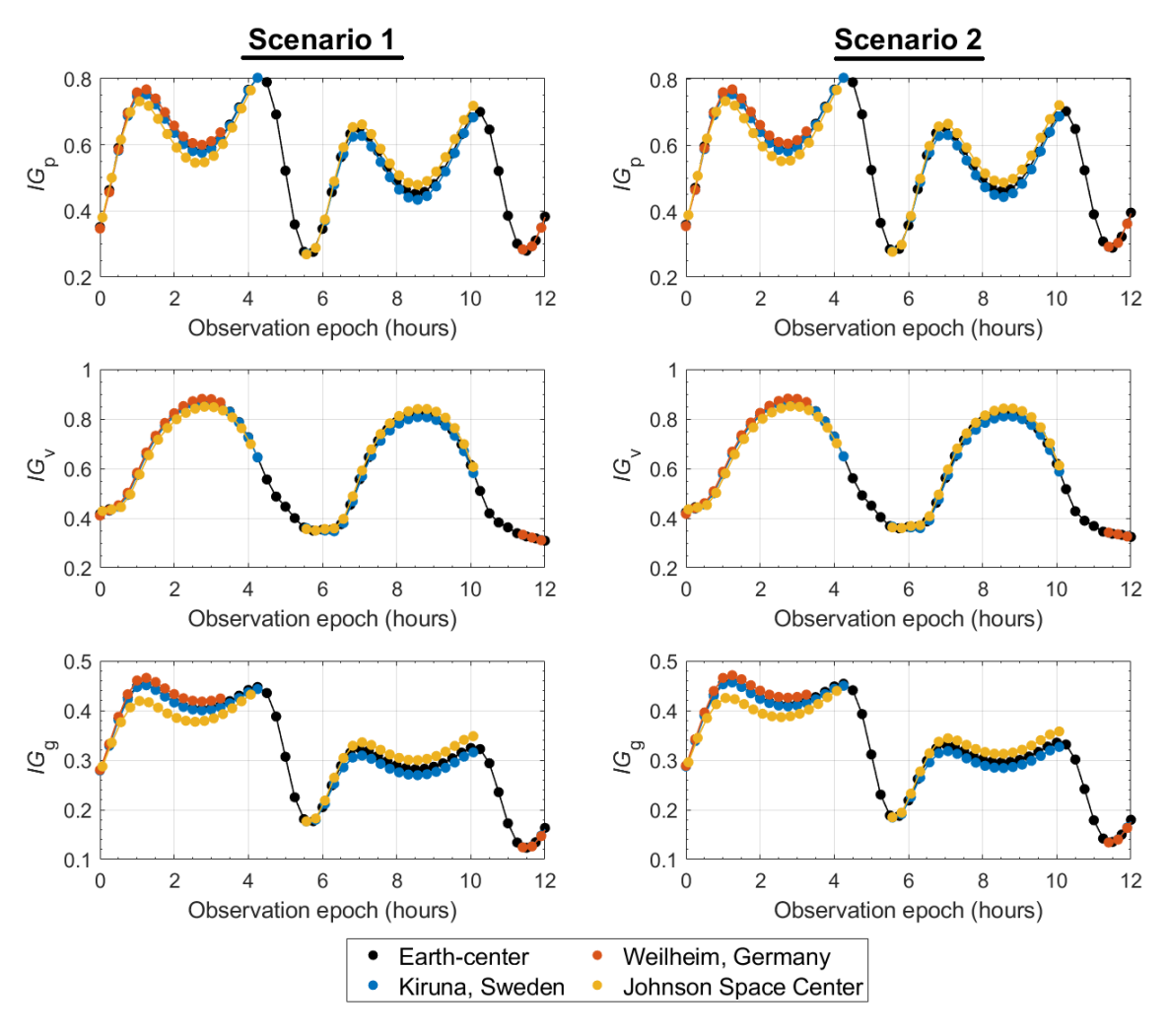


Figure 7. Orbit 1 information-gain measures

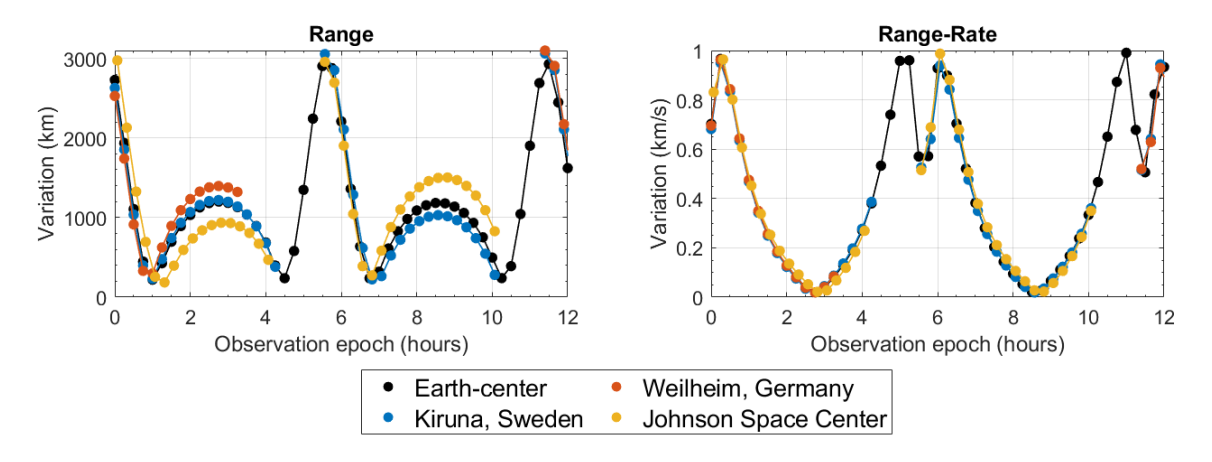


Figure 8. Orbit 1 range and range-rate variations

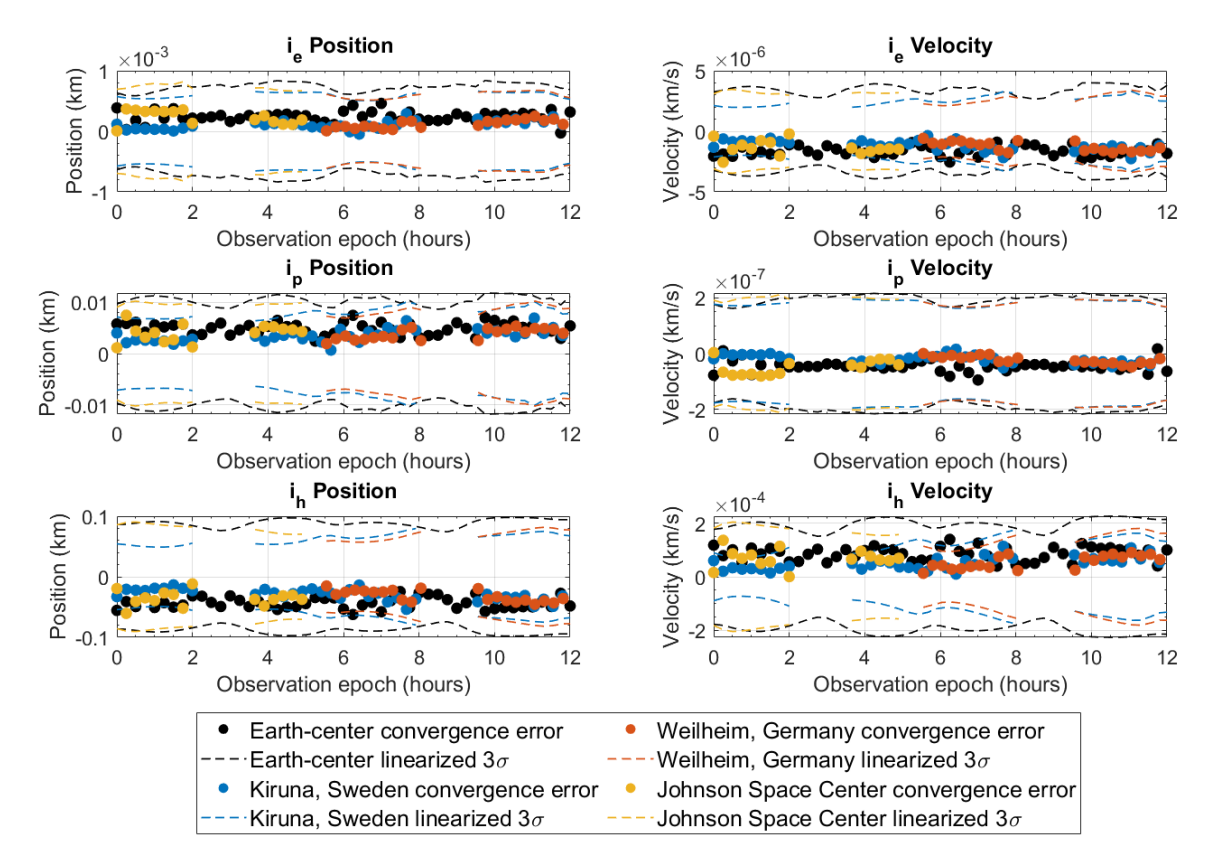


Figure 9. Orbit 2 convergence error and linearized  $3\sigma$  uncertainty bounds

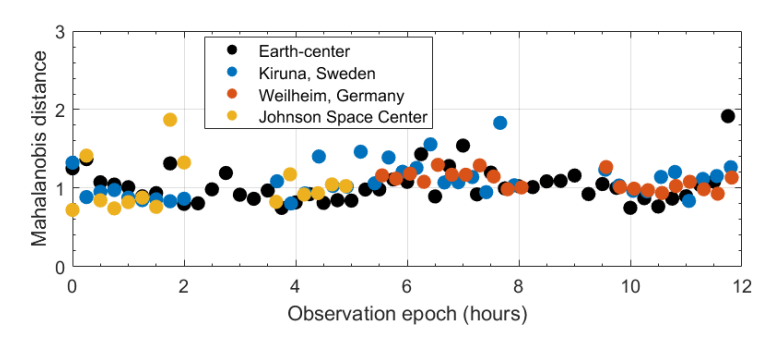


Figure 10. Orbit 2 Mahalanobis distance

linearized  $3\sigma$  bounds with slight bias in the convergence error. Compared to Orbit 1, Orbit 2 is seen to have significantly more difference in the uncertainty profiles between each observation locations. This indicates greatly varying levels of observability between each observation location, which was not seen when performing the analysis on Orbit 1. It is expected that this is due to the comparatively larger uncertainty of *a priori* information in Orbit 2, leading to the observability of the problem depending more on the observation location. Despite the differences in observability, the Mahalanobis distance of the *a posteriori* epoch state estimates for Orbit 2 (figure 10) are seen to behaving with statistical consistency. This, once again, indicates the accuracy of the *a posteriori* epoch state and uncertainty information.

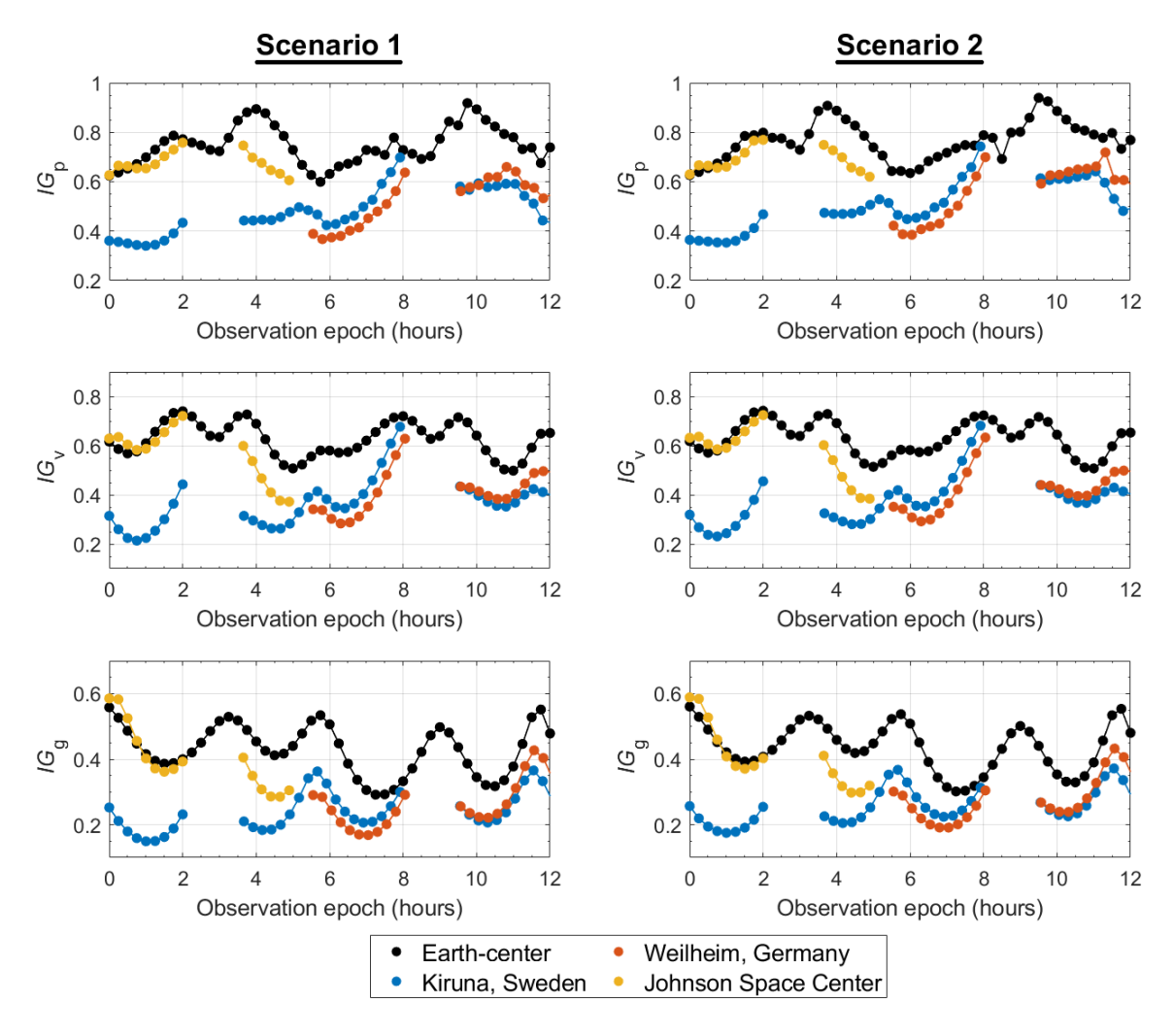


Figure 11. Orbit 2 information-gain measures

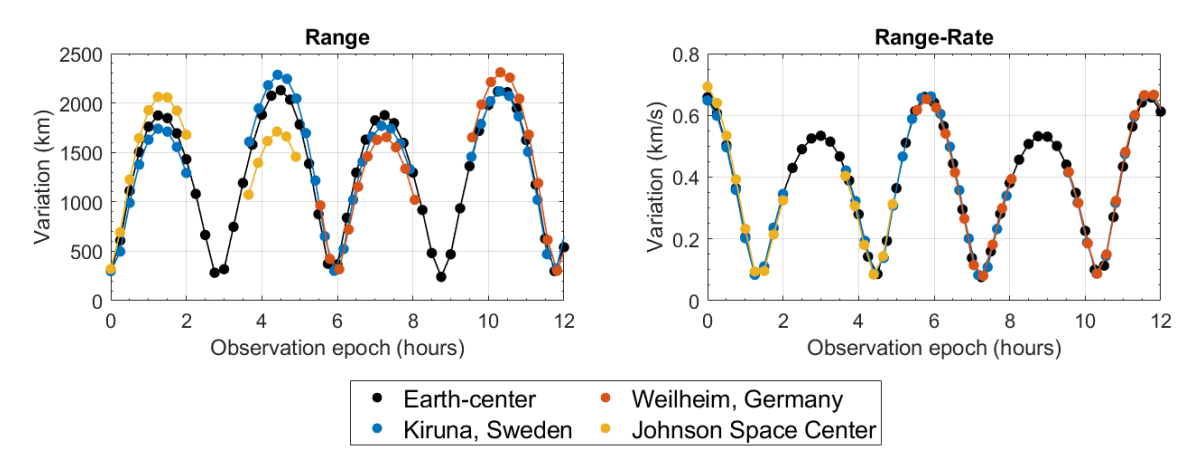


Figure 12. Orbit 2 range and range-rate variations

Figure 11 reveals the information-gain measures as a function of the observation epoch for Orbit 2. As expected, each information-gain measure reveals significant variations between each observation location and observation epoch. However, information-gain profiles are near identical between both scenarios. This further bolsters the efficacy of the work presented in this paper, revealing that the analysis method presented here is a useful tool to plan the optimal satellite observation times. While the variations of range and range-rate of figure 12 can be seen to influence the information-gain, they are significantly less influential when compared to Orbit 1. Not only do the shapes of the information-gain profiles vary between observation location, but the profile magnitudes at the same observation epoch vary significantly as well. This, once again, heavily implies that observation location variation plays a significant role in the observability of Orbit 2. Due to the significant non-linearity of the problem, it is difficult to determine what effects of the ground-based sites are driving these trends. Thus, performing this ground-based site analysis during mission planning is needed to determine the optimal observation epoch when the target orbit has significant uncertainty in the *a priori* estimate.

# **CONCLUSIONS**

A non-linear batch least squares algorithm is presented in this paper to study the sensitivity of the epoch state orbit determination problem in the cis-lunar domain. Representative dynamics and sensor models are developed to provide the range and range-rate observations utilized to estimate the epoch state. First order partial derivatives of the perturbing effects are used to track the state transition matrix that maps the sensitivity of the epoch position-velocity state to the position-velocity state at the time of observations. The state transition matrix is used to populate the *Jacobian* matrix of the batch estimator, providing an increased computational efficiency of the Jacobian over standard numerical differentiation methods. The sensitivity analysis is performed on two example lunar orbits, one near-circular equatorial orbit and one eccentric polar orbit. The statistical consistency of the batch estimation algorithm is verified by calculating Mahalanobis distance and comparing the epoch state residuals to the epoch state uncertainty. Information-gain measures are presented to reveal optimal observation times and the uncertainty sensitivities to ranging geometry and observation location. Measurement variation is seen to drive the epoch state observability when the uncertainty of the a priori epoch state uncertainty is near the minimum achievable in the lunar domain. Observation location variation is seen to have significant influence on observability when the a priori epoch state uncertainty is an order of magnitude greater than what is achievable. Information-gain measures were seen to be near identical between measurements generated from a true epoch state and an a priori epoch state, indicating the effectiveness of this analysis for mission and operation planning.

# **ACKNOWLEDGEMENTS**

The authors appreciate Davis Adams, Dr. Eric Anderson, Dr. Alok Das, and Dr. John Junkins for their suggestions.

# REFERENCES

- [1] R. Kalman, "A new approach to linear filtering and prediction problems," *ASME Journal of Basic Engineering*, Vol. 82, 1960, pp. 35–45. Series D.
- [2] B. D. O. Anderson and J. B. Moore, *Optimal filtering / Brian D. O. Anderson, John B. Moore*. Prentice-Hall, Englewood Cliffs, N.J.:, 1979.

- [3] A. H. Jazwinski, Stochastic processes and filtering theory [by] Andrew H. Jazwinski. Academic Press, New York., 1970.
- [4] T. Kailath, A. H. Sayed, and B. Hassibi, *Linear Estimation*. Upper Saddle River, NJ: Prentice Hall, 2000.
- [5] J. L. Junkins, "Adventures in the interfaces of dynamics and control," *Journal of Guidance, Control, and Dynamics*, Vol. 29, No. 6, 1997, pp. 1058–1071.
- [6] J. L. Junkins and P. Singla, "How Nonlinear Is It?," *The Journal of Astronautical Sciences*, Vol. 52, No. 1-2, 2003, pp. 7–60.
- [7] D. J. Kessler and B. G. Cour-Palais, "Collision Frequency of Artificial Satellites: The Creation of a Debris Belt," *Journal of Geophysical Research*, 1978.
- [8] D. Izzo, "Statistical Disribution of Keplerian Velocities," *Journal of Guidance, Control, and Dynamics*, Vol. 20, No. 6, 2006, pp. 298–395.
- [9] M. Majji, J. Junkins, and J. Turner, "A High Order Method for Estimation of Dynamic Systems," *The Journal of the Astronautical Sciences*, Vol. 56, 09 2008, 10.1007/BF03256560.
- [10] R. Weisman, M. Majji, and K. T. Alfriend, "Solution of Liouville's Equation for Uncertainty Characterization of the Main Problem in Satellite," *Tech Science Press CMES*, Vol. 111, No. 3, 2016, pp. 269–304.
- [11] M. Majji, J. L. Junkins, and J. D. Turner, "A Perturbation Method for Estimation of Dynamic Systems," Nonlinear Dynamics, Vol. 60, No. 3, 2010, pp. 303–325.
- [12] M. J. Holzinger, D. J. Scheeres, and J. Hauser, "Reachability Using Arbitrary Performance Indices," IEEE Transactions on Automatic Control, Vol. 60, No. 4, 2014, pp. 1099–1103.
- [13] B. Jones, A. Doostan, and G. H. Born, "Nonlinear Propagation of Orbit Uncertainty Using Non-Intrusive Polynomial Choas," *Journal of Guidance, Control, and Dynamics*, Vol. 36, No. 2, 2013, pp. 430–444.
- [14] K. T. Alfriend, "Continuing Kepler's Quest: Assessing Air Force Space Command's Astrodynamics Standards," the national academies press, National Research Council, Washington, D. C., 2012.
- [15] M. Majji, J. L. Junkins, and J. D. Turner, "A High Order Method for Estimation of Dynamic Systems," Journal of Astronautical Sciences, Vol. 56, No. 3, 2008, pp. 401–440.
- [16] J. L. Crassidis and J. L. Junkins, Optimal Estimation of Dynamic Systems. CRC Press/Chapman Hall, 2014.
- [17] A. Gelb, J. F. Kasper, R. A. Nash, C. F. Price, and A. A. Sutherland, Applied Optimal Estimation. The Analytical Sciences Corporation, The M.I.T. Press, 1974.
- [18] R. G. Gottlieb, "Fast gravity, gravity partials, normalized gravity, gravity gradient torque and magnetic field: derivation, code and data," 1993.
- [19] S. E. Slojkowski, J. Lowe, and J. A. Woodburn, "Orbit Determination for the Lunar Reconnaissance Orbiter Using an Extended Kalman Filter," 2015.
- [20] E. Mazarico, D. Rowlands, G. Neumann, D. Smith, M. Torrence, F. Lemoine, and M. Zuber, "Orbit determination of the lunar reconnaissance orbiter," *Journal of Geodesy*, Vol. 86, No. 3, 2012, pp. 193–207.
- [21] E. Mazarico, G. A. Neumann, M. K. Barker, S. Goossens, D. E. Smith, and M. T. Zuber, "Orbit determination of the Lunar Reconnaissance Orbiter: Status after seven years," *Planetary and Space Science*, Vol. 162, 2018, pp. 2–19. Lunar Reconnaissance Orbiter Seven Years of Exploration and Discovery, https://doi.org/10.1016/j.pss.2017.10.004.
- [22] D. Mao, M. Torrence, E. Mazarico, X. Sun, D. Rowlands, J. McGarry, G. Neumann, M. Barker, J. Golder, D. Smith, *et al.*, "LRO orbit determination with laser ranging data," *18th International Workshop on Laser Ranging*, Hitotsubashi Univ. Fujiyoshida, Japan, 2013.